Article

The Effect of Superabsorbent Polymers on the Microstructure and Self-Healing Properties of Cementitious-Based Composite Materials

Irene A. Kanellopoulou, Ioannis A. Kartsonakis [ID] and Costas A. Charitidis *[ID]

School of Chemical Engineering, R-Nano Lab, Laboratory of Advanced, Composite, Nanomaterials and Nanotechnology, National Technical University of Athens, 9 Heroon Polytechniou str., Zografou Campus, 15773 Athens, Greece; ikan@chemeng.ntua.gr (I.A.K.); ikartso@chemeng.ntua.gr (I.A.K.)

* Correspondence: charitidis@chemeng.ntua.gr; Tel.: +30-210-772-4046

Featured Application: Superabsorbent polymers of novel structure have been used in cementitious-based composite materials improving their self-healing behavior by an index of 60%.

Abstract: Cementitious structures have prevailed worldwide and are expected to exhibit further growth in the future. Nevertheless, cement cracking is an issue that needs to be addressed in order to enhance structure durability and sustainability especially when exposed to aggressive environments. The purpose of this work was to examine the impact of the Superabsorbent Polymers (SAPs) incorporation into cementitious composite materials (mortars) with respect to their structure (hybrid structure consisting of organic core—inorganic shell) and evaluate the microstructure and self-healing properties of the obtained mortars. The applied SAPs were tailored to maintain their functionality in the cementitious environment. Control and mortar/SAPs specimens with two different SAPs concentrations (1 and 2% bwoc) were molded and their mechanical properties were determined according to EN 196-1, while their microstructure and self-healing behavior were evaluated via microCT. Compressive strength, a key property for mortars, which often degrades with SAPs incorporation, in this work, practically remained intact for all specimens. This is coherent with the porosity reduction and the narrower range of pore size distribution for the mortar/SAPs specimens as determined via microCT. Moreover, the self-healing behavior of mortar-SAPs specimens was enhanced up to 60% compared to control specimens. Conclusively, the overall SAPs functionality in cementitious-based materials was optimized.

Keywords: mechanical properties; microstructure; self-healing; SAP; microCT; cementitious materials; mortar

1. Introduction

Cementitious materials have been widely used over the years in the construction sector due to the cement abundance, its low cost and excellent durability [1,2]. In 2017 the global cement production came up to 4.1 billion tones. China and India which currently represent two of the most rapidly growing countries worldwide produced 57% and 7% of the global cement production in that year, while 6% of the same production is attributed to Europe [3]. It is estimated that the cement production will double in the decades to come [2,4].

Nevertheless, cement is prone to cracking as a result of both inherent material properties such as low tensile strength and application related factors such as tension inducement during the infrastructure service life thus compromising its integrity and durability [1,5–7]. Aggressive environment conditions (i.e., wide ambient temperature fluctuation, rich presence of ions, pH levels etc.) combined with external loading favor crack propagation often leading to the formation of an interconnected crack network that allows corrosive factors to

penetrate the structure and assault the reinforcement thus leading to its deterioration. This raises huge safety issues and makes maintenance and repair high priority concerns [6–8].

Even though autogenous crack self-healing in cementitious materials has been known for centuries, its effectiveness highly depends on numerous factors, namely the crack width and age, water abundance upon the crack formation, environment conditions such as pH and presence of ions etc. [6,9–11]. Conventional retrofitting/repair methods applied up to now mainly consist of textile reinforced mortar/concrete (TRM/TRC), the textiles used mainly being based on carbon, glass and aramid fibers, polymer crack injection and polymer modified concrete [1,9,10]. These methods have proven to be effective but in several cases, the cost is prohibitive and/or these methods are difficult or even impossible to apply because of the location of the damaged spot on the infrastructure [6,9].

As a result, internal curing promoting methods have gained a lot interest in the last two decades [1,9]. These methods focus on (i) maintaining continuous water provision and thus continuous cement hydration and (ii) restraining cement self-desiccation [1]. Over the years, the incorporation of several internal curing agents in cementitious materials such as Light Weight Aggregates (LWA) [1,2,5,9,12,13], Superabsorbent Polymers (SAPs) [9,10,14–26], Rice Husk Ash (RHA) [1,5,27], bottom ash [1,5,28], fly ash [1,2,5,9,13,29], cenospheres [1,5,30], crushed returned concrete fine aggregates (CCA) [1,13] and wood fibers [1,13] has been tested. In this application field, SAPs seem to have very promising results and gain more research interest [10].

The SAPs are 3-D polymer networks that due to their hydrophilic nature absorb huge amounts of water (even thousands of times their own dry weight), while due to the network crosslinking they retain their structure and are not dissolved [1,14,15,19,22,24,31]. It is confirmed that their total water absorption level is inversely dependent on environment related factors such as the presence of ions and pH values [10,18,22,24].

Due to their properties, SAPs are used in a vast variety of applications such as hygienic products, agriculture, drug delivery systems, sealing, pharmaceuticals, biomedical applications, tissue engineering, biosensors and the construction field [32]. In the construction field, attention has been drawn to different strategies to obtain coatings with debonding properties [33]. One of these strategies is to incorporate SAPs into an intermediate primer layer between the substrate and the top coatings. The trigger mechanism relies on the fact that with a pH variation, the SAPs can enhance their shape due to the water absorption resulting in the reduction of the attachment between the primer layer and both the top coating and substrate, enabling the detachment of the top coating from the corresponding substrate. Moreover, in cementitious pastes a large number of ions are present (Ca^{2-}, K^+, Na^+, SO_4^{2-}, OH^- etc.) and pH of the mix water ranges between 11 and 13.4 [10,15,22,24,34].

The incorporation of SAPs in cementitious materials initially results in water absorbance during the cement paste mixing procedure and act as water reservoirs that will make water available during cement curing and hardening. In this way, SAPs contribute to maintaining higher levels of relative humidity thus mitigating early age shrinkage and at the same time favoring extended hydrating reactions which lead to denser cement microstructure by reducing the capillary pores in the cementitious matrix which leads to improved structure strength [9,10,15–17,20,23,24]. Furthermore, upon crack formation and in the presence of water, SAPs reabsorb water on a separate event, swell and allow an immediate crack self-healing effect while the promotion of additional hydrating reactions of remaining unhydrated cementitious phases provide a crack self-healing effect, thus acting as internal curing agents [9–11,14–17,23]. On the other hand, when water is released from SAPs particles in the cement matrix, SAPs deswell forming voids around them in the scale of macropores. These macropores are likely to act as strain inducers and be accounted for any strength loss detected in the final structure, a competitive effect to the internal curing promotion that was previously described [9,10,15,17,21,31,35].

It must be clarified that the overall SAPs behavior in cementitious materials highly depends on the nature of SAPs used and their characteristics such as structure, absorp-

tion/desorption behavior, morphology (particles shape, size and size distribution) and dosage in the cementitious matrix, as well as water to cement (w/c) ratio and the incorporation procedure adopted [9,15,17,31,35]. In most cases SAPs absorption/desorption has been examined in extracted or synthetic solutions. Nevertheless, there have also been some studies on the in-situ evaluation of this behavior when SAPs are incorporated in a porous cementitious matrix. The results from these studies revealed that SAPs desorption when in contact with a porous, cementitious material, is effected by the bonding between SAPs particles and the cementitious matrix and is governed by diffusion between SAPs particles and capillary sorption in the matrix [36–38]. Consequently, it is imperative to investigate the correlation between SAPs used and the response of the cementitious system with respect to its mechanical properties and its microstructure.

The vast majority of commercial SAPs are copolymeric networks based on acrylic acid or acrylamide that may or may not have been partially neutralized [10,11,14,15,17,18,20–23,31,35]. Because of the diversity of the parameters that have to be satisfied in the construction applications to enhance their internal curing action, SAP particles should preferentially have a homogeneous spherical shape, size in the submicron area so that the voids left behind after their deswelling are smaller and don't affect the structure mechanical properties and chemical affinity to the cement matrix so that they are more easily dispersed homogeneously in the cement paste [23].

The aim of this work was to examine the impact of the incorporation of tailored SAPs with respect to their structure (hybrid structure consisting of organic core—inorganic shell) on mortars mechanical strength in terms of flexural and compressive strength, microstructure and self-healing behavior. The synthesis and characterization of the incorporated SAPs have been thoroughly discussed in previous authors' work. More specifically, the SAP particles used were spherical in the submicron range based on poly (methacrylic acid) crosslinked with ethylene glycol dimethacrylate which were synthesized via radical polymerization and later encapsulated with CaO-SiO$_2$ inorganic shell via the sol-gel method [25,39]. The incorporation of SAPs in mortars was conducted in two different dosages, 1% and 2% by weight of cement (bwoc). The results obtained in this work revealed that the flexural strength improved by 3%, while the compressive strength remained practically intact for the mortar/SAP composite materials compared to the control specimens. Moreover, the total and closed porosity of the mortar/SAPs specimens were reduced by about 0.5% and 2.5% for mortar-SAPs-1 and mortar-SAPs-2, respectively, while self-healing behavior was enhanced for both SAPs concentrations (in the case of mortar-SAPs-1 by 60% and in the case of mortar-SAPs-2 by 10% compared with mortar-reference specimens).

The added value of this work resides in the optimization of the SAPs functionality in cementitious-based materials and the improvement of the cementitious materials self-healing properties due to tailored SAPs structure, which are easy to fabricate via the combination of the sol-gel process, radical polymerization and the coprecipitation method. Finally, a new approach for the quantitative evaluation of mortars self-healing behavior was proposed.

2. Materials and Methods

2.1. Materials

Sand grade in accordance to CEN, EN 196-1 standard, cement CEM I 52.5 N and in-house synthesized SAPs were used to manufacture conventional mortar specimens. As mentioned earlier, the SAPs used were synthesized according to previous authors' work [39]. In Figure 1 the novel SAPs structure which consists of a hybrid organic core of poly(methacrylic acid) crosslinked with ethylene glycol dimethacrylate encapsulated with a composite inorganic shell of silicon-calcium oxide, P(MAA-co-EGDMA)@CaO-SiO$_2$ (Figure 1a,b) is shown. Their size ranges from 190 to 320 nm (Figure 1c) while their maximum water absorbance ratio in cement slurry filtrate is determined 1100% their initial dry weight. Before their incorporation in mortars, SAPs are ground to fine powder form, in order to dismantle agglomerates and enhance their performance.
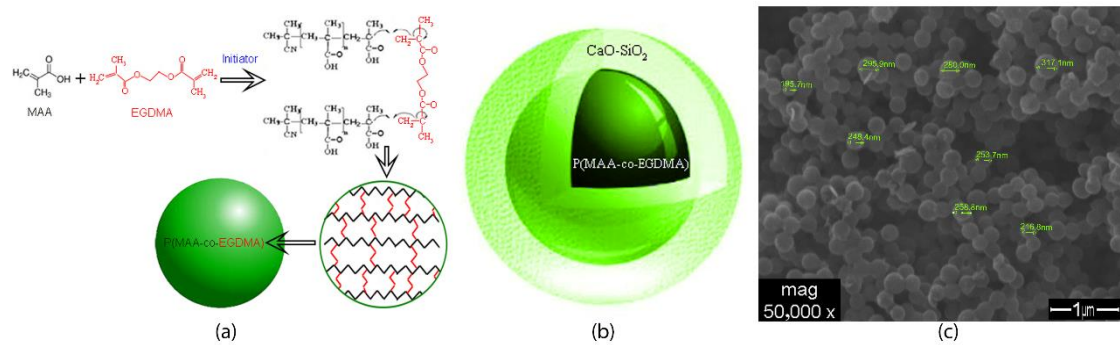
Figure 1. Polymerization reaction to form the organic core P(MAA-co-EGDMA (**a**), schematic representation of organic core—inorganic shell (**b**), SEM image of the synthesized SAPs/P(MAA-co-EGDMA)@CaO-SiO$_2$ (**c**), revealing the homogenous spherical morphology of SAPs particles in the nanoscale.

2.2. Methods

2.2.1. Manufacture of Mortar/SAPs Specimens

Two specimen series of mortar/SAPs composites were manufactured, prismatic and cylindrical. Prismatic test specimens were fabricated according to the EN 196-1 [40] using a Teflon mold, while cylindrical specimens were using a medical disposable syringe [41–43]. The specimens were cast from a batch of mortar paste with a water/cement ratio (w/c) of 0.50. In accordance to literature review and previous authors' work on cement/SAPs composites [7,10,11,15,16,20,21,23,31,35,39], SAPs were incorporated in mortar in two different dosages, 1 and 2% by weight of cement (bwoc). The SAPs incorporation in the mortar paste was accomplished in succession to the sand fraction and the obtained mortar paste was mixed until the visually monitored dispersion was acceptable. In all cases mixing time needed was more than 30 s. A mortar mixer (MATEST-E094) was used for the dry mechanical mixing of the mixture components and a jolting apparatus (MATEST-E130) to compact the specimens. The molded samples were stored in the moist air room for 24 h and after demolding they were submerged horizontally in a suitable container at 20 °C for 28 days. The composition of the specimens is shown in Table 1.

Table 1. Composition of the mortar specimens.

	Cement (g)	Sand (g)	Water (g)	SAPs (g)
Mortar-reference	450	1350	225	0.0
Mortar-SAPs-1	450	1350	225	4.5
Mortar-SAPs-2	450	1350	225	9.0

2.2.2. Mechanical Properties of Mortar/SAPs Specimens

The flexural strength of mortar/SAPs composites was evaluated using prism specimens with dimensions 40 mm × 40 mm × 160 mm according to EN 196-1 using a universal testing machine of capacity 300 KN (Instron 300DX-B1-C4-G6C) [40]. For each SAPs dosage as well as for control samples, triplicates were manufactured, demolded and tested after 28 days curing in water. The prism halves from the flexural strength tests were used for the compressive strength tests, which were also performed according to EN 196-1.

2.2.3. Microstructure of Mortar/SAPs Specimens

X-ray micro computed tomography (microCT) was utilized to evaluate the mortar/SAPs composites microstructure. This technique is based on the correlation between X-rays absorption, material density and atomic number. High-density materials absorb X-rays more profoundly and produce light grey projection images. On the other hand, low-density materials are visualized as darker projection images. During the scanning process, angular projections of the specimen were acquired and saved. After the angular

projections acquisition was completed, their reconstruction followed. The reconstruction process was executed by the "NRecon" visualization program via the implementation of Feldkamp algorithm. As a result, a 3D reconstructed model of the scanned specimen was produced. Moreover, quantitative parameters were determined using densiometry and morphometry evaluation, the latter based on image segmentation (black and white) which was done via a global threshold method, the Otsu method [44].

In this work, the specimens were scanned using SkyScan 1272 X-ray micro-tomograph at the age of 28 days. The specimens' geometry was chosen to be cylindrical; their diameter was 10 mm and their height ranged between 20 and 30 mm. In order to enhance contrast in microCT images and improve grey scale histogram segmentation iodine was utilized as a contrast agent. Therefore, all specimens were treated with a 3% iodine solution in ethanol prior to their scans. More specifically, at the age of 28 days, the cylindrical specimens were submerged in the iodine solution for 48 h and then, they were dried in an oven at 80 °C for 24 h. If the specimens were not immediately scanned, they were stored in a desiccator [45]. The acquisition settings of the scans are presented in Table 2. In addition, for each scan the flat field correction was applied.

Table 2. Acquisition settings of the X-ray micro-tomography scans.

Acquisition Settings		Value
Source Voltage	kV	60
Source Current	uA	120
Image Pixel Size	um	9
Filter		Al 0.5 + Cu 0.038
Rotation Step	deg	0.2
Rotation	deg	180

The reconstruction and the porosity analysis were performed using NRecon (version 1.6.6.0) and CTAnalyzer (version 1.13) softwares, respectively. The selected volumes of interest were 441, 105 and 350 mm^3 for mortar-reference, mortar-SAPs-1% and mortar-SAPs-2%, respectively. Figure 2 shows representative 2D and 3D reconstructed images of the scanned specimens ((a), (b) mortar-reference; (c), (d) mortar-SAPs-1%; (e), (f) mortar-SAPs-2%).
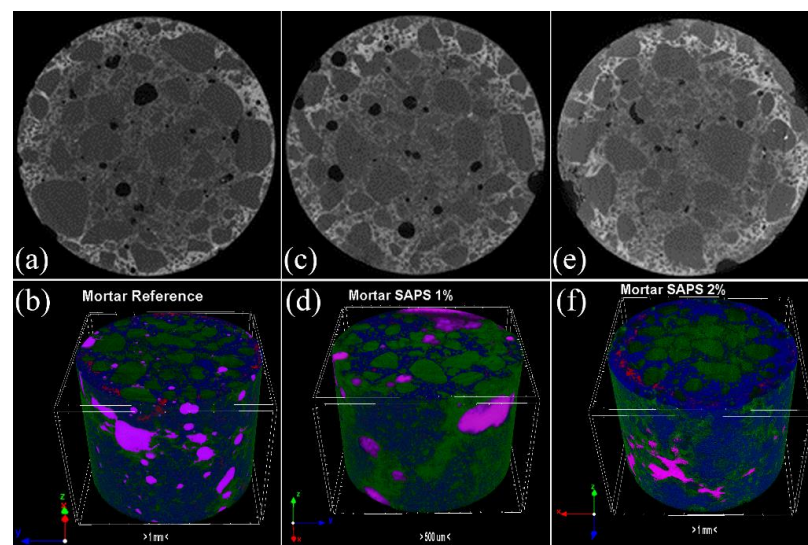

Figure 2. 2D and 3D reconstructed images of the scanned specimens of: mortar-reference (**a**,**b**); mortar-SAPs-1% (**c**,**d**); mortar-SAPs-2% (**e**,**f**).

Moreover, the challenging issues of material phase segmentation and their quantitative analysis were addressed via 2D and 3D reconstructed images data, and more specifically

via the grey scale intensity thresholds. In particular, even though microCT does not support chemical analysis, differences in brightness are recorded in the form of Grey Scale Histograms (GSH) due to density and atomic mass variations for different materials. As a result, phase segmentation depends on the thresholding method followed in each case [46]. In this work, GSH were obtained during the scan data processing via CTAnalyzer Software. The Grey Scale Values ranged from "0" to "255". The lower grey scale values correspond to black color in reconstructed images and were attributed to the lack of material or pores. On the other hand, the higher values correspond to white and were attributed to unhydrated cement phases and/or SAPs aggregates, while the intermediary grey scale values are depicted as grey and were attributed to different hydrated cement phases [44,46–50]. In this work, taking into consideration that all hydrated cement phases, mainly Calcium Silicate Hydrates(C-S-H) are expected to show peaks at similar grey scale values, a deconvolution procedure was engaged to identify and quantify the different material phases (pores, hydrated cement phases, unhydrated cement phases and SAPs) assuming that the grey scale values distribution for each phase is Gaussian. Then, a fitting model distribution, comprising a set of four (n = 4) Gauss distributions was numerically fitted to the GSH using an algorithm implemented in Software "Magic Plot" (student version 2.5.1).

2.2.4. Self-Healing Evaluation of Mortar/SAPs Specimens

Cementitious structures can be damaged in a variety of ways, the most common being cracking. MicroCT has been utilized as a laboratory-scale method to evaluate their damage extent and interpret healing mechanisms. In the past more conventional methods, such as SEM (Scanning Electron Microscopy), have been used to evaluate crack morphology and mitigation but they can provide insight only on the specimen surface, whereas microCT can provide useful information on the bulk of the specimen and consequently evaluate internal cracks and internal self-healing [46].

In this work, after 28 days of curing the cylindrical specimens that were previously examined via microCT were precracked under compressive load using a hydraulic press. During their compression, the load was applied in a controlled and smooth manner but the specimens were completely split in two halves in all cases. Therefore, prior to this procedure they were wrapped tightly in a polypropylene based film in order to avoid the complete separation of the two halves but instead to form a crack as shown in Figure 3. Afterwards, the specimen circumference and base were coated with an epoxy resin (a mixture of Sinmast J 158 (component A) and Sinmast S2 liquid primer (component B) by Sintecno in a ratio A:B 77:23) in order to secure the two halves together. The top surfaces of the cylinders were untreated, so that the formed crack could interact with healing agents (water). The epoxy resin was cured at ambient temperature for 1 day and then at 60 °C for 2 h.
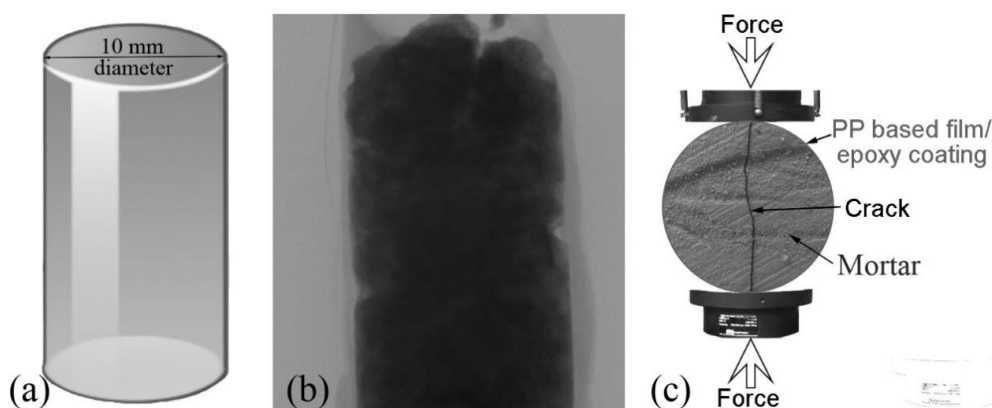

Figure 3. Schematic representation of mortar cylinder (**a**), specimen image from microCT CCD camera (**b**), crack inducement in cylindrical specimens via compression load enforcement (**c**).

In order to estimate their self-healing behavior, the cracked specimens were submerged in water at ambient temperature and they were evaluated at different time slots (0 and 8 days). The self-healing efficiency of mortar/SAPs composites was quantified and visualized via microCT analysis. Prior to microCT evaluation the specimens were dried at 50 °C for three days and were stored in a desiccator. The cracked mortar specimens were scanned using the SkyScan 1272 desktop microCT at 25.0 μm pixel resolution with 0.5 mm aluminum filter. The scanned images were reconstructed via NRecon software, while three-dimensional evaluation was conducted by CTAnalyzer software following a methodology proposed by Nicole Y.C Yu et al., appropriately adjusted for cracked mortar specimens [51]. The main outcomes discussed in this work were the evolution of connectivity density and the percent object volume versus healing time. These parameters were adopted because they allow the quantitative evaluation of crack healing in 3D (not only in 2D), with respect to crack closure in terms of changes in morphology and density and are embedded in the CTAnalyzer software.

3. Results

3.1. Mechanical Properties of Mortar/SAPs Specimens

During the flexural strength test an abrupt, brittle failure was observed in mortars mainly due to deformation localization by the coalescence of narrow microcracks that ultimately lead to macrocracks that expand to the entire specimen [52]. The flexural strength evaluation of the mortar-based composites with SAPs in dosages 1 and 2% bwoc as well as control mortar specimens at the age of 28 days is demonstrated in Figure 4a,b. According to Figure 4b, a slight increment of about 3% can be detected on the flexural strength of the mortar-based composites that contain SAPs in dosages 1% and 2% bwoc, in comparison to the control specimens which practically reveals that the flexural strength remains intact after the SAPs incorporation in both concentrations.
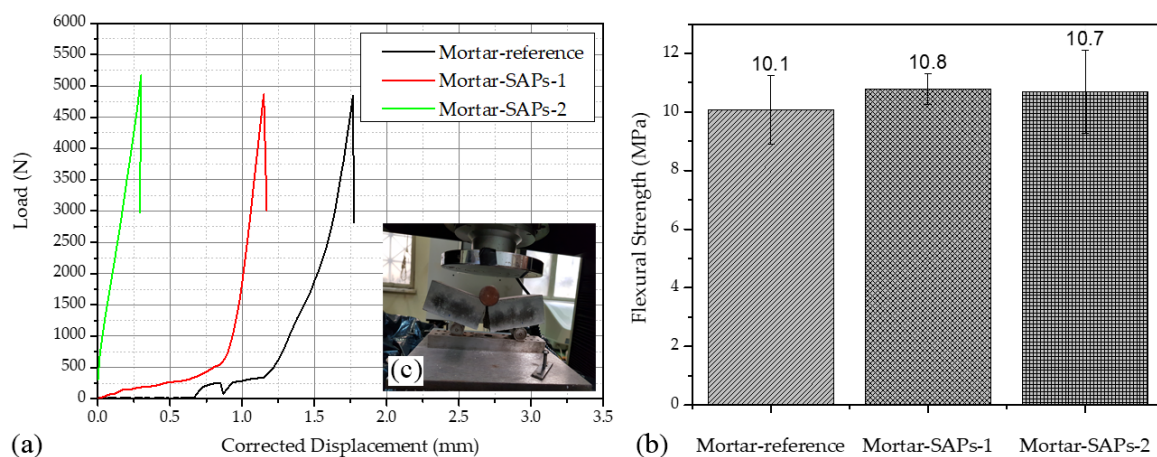

Figure 4. Maximum values of loads for mortar specimens at 28 days of age (**a**), flexural strength of mortar specimens at 28 days of age (**b**), optical image of specimen after flexural test (**c**).

On the other hand, the compressive strength of the mortar based composite materials with the SAPs incorporation for the same mortar age (28 days) and w/c ratio (0.5) is depicted in Figure 5a,b. More specifically, Figure 5a depicts the load applied during the test as a function of the head displacement and Figure 5b shows the calculated compressive strength of the mortar based composite materials with the SAPs incorporation for the same mortar age (28 days) and w/c ratio (0.5). As shown in Figure 5b the compressive strength of the mortar-based composite materials practically remains intact for both SAPs dosages (1% and 2% bwoc) in comparison with the control materials.
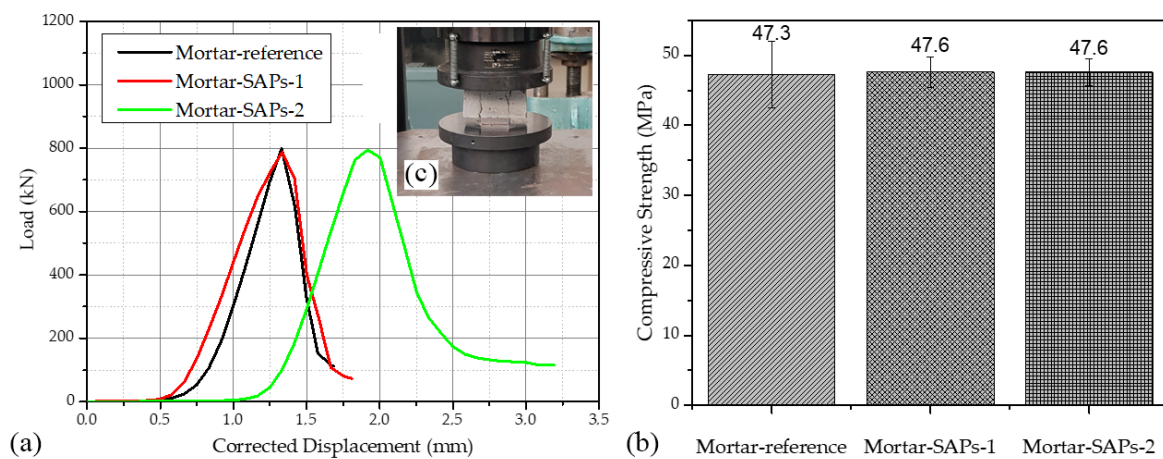
Figure 5. Maximum values of loads for mortar specimens at 28 days of age (**a**), compressive strength of mortar specimens at 28 days of age (**b**), optical image of specimen after compressive test (**c**).

Figure 6 reveals the relationship between the flexural and compressive strength of the mortar-based control and composite materials using the corresponding average values at the age of 28 days. It can be observed that a direct relationship ($R^2 = 0.97818$) between them exists. Similar behaviors have been reported by other research works for reference mortars [53,54].
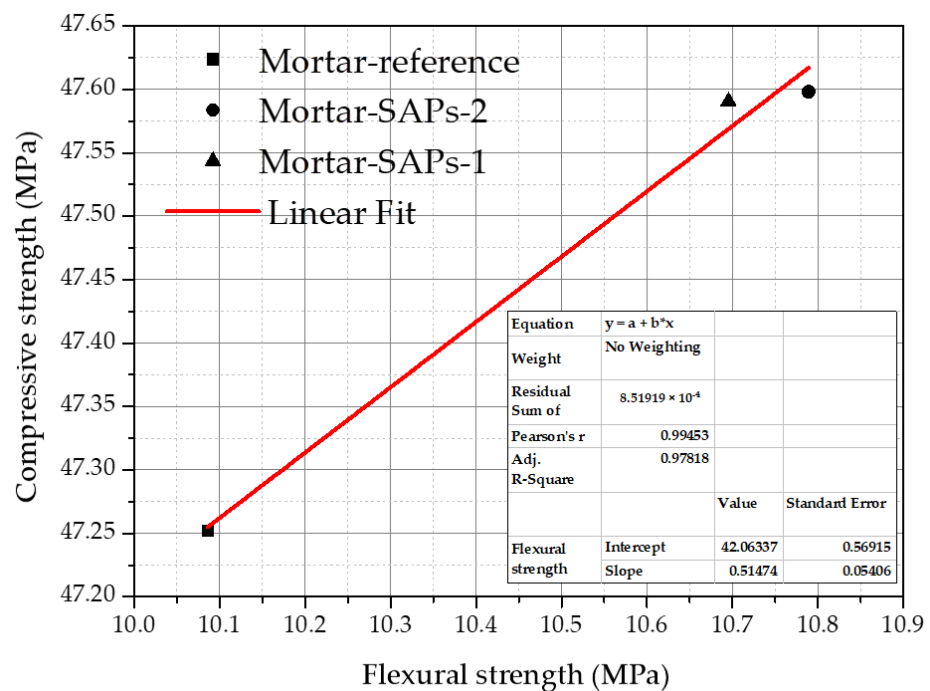

Figure 6. Relationship between compressive and flexural strength of mortar-based materials.

3.2. Microstructure of Mortar/SAPs Specimens

3.2.1. Microstructure Analysis

In this work, the effect of SAPs incorporation on the mortar microstructure in means of porosity and phase segmentation was examined via microCT. In cementitious materials, porosity affects greatly key properties such as mechanical and transport properties [46]. Moreover, the dispersion quality of SAPs in the cementitious matrix can be evaluated through porosity determination. The porosity of cementitious materials is usually divided into gel pores (ranging from a few nanometers to 0.2 µm), capillary pores (ranging from

0.2 to 10 μm), and air voids (above 10 μm) [50,55,56]. In this work, the pore analysis from micro-CT applies only to the pores with diameters larger than 9 μm. The specimen size dictates the minimum distance that can be reached from the X-ray source during scanning and consequently the accuracy of the method. Therefore, the pore analysis from micro-CT scans includes partially capillary pores and the air voids. Air voids are mainly of interest in this work, as in literature, it is reported that the incorporation of SAPs in cementitious matrixes creates air voids around them as a result of the water absorption/desorption by them combined with their poor dispersion in cement and therefore the formation of large SAPs agglomerates [9,10,15,21,31,35,38]. The statistical pore analysis of mortar specimens and the corresponding pore size distribution are exhibited in Table 3 and Figure 7, respectively. The statistical pore analysis parameters calculated are delineated as follows.

Table 3. Statistical pore analysis of mortar specimens.

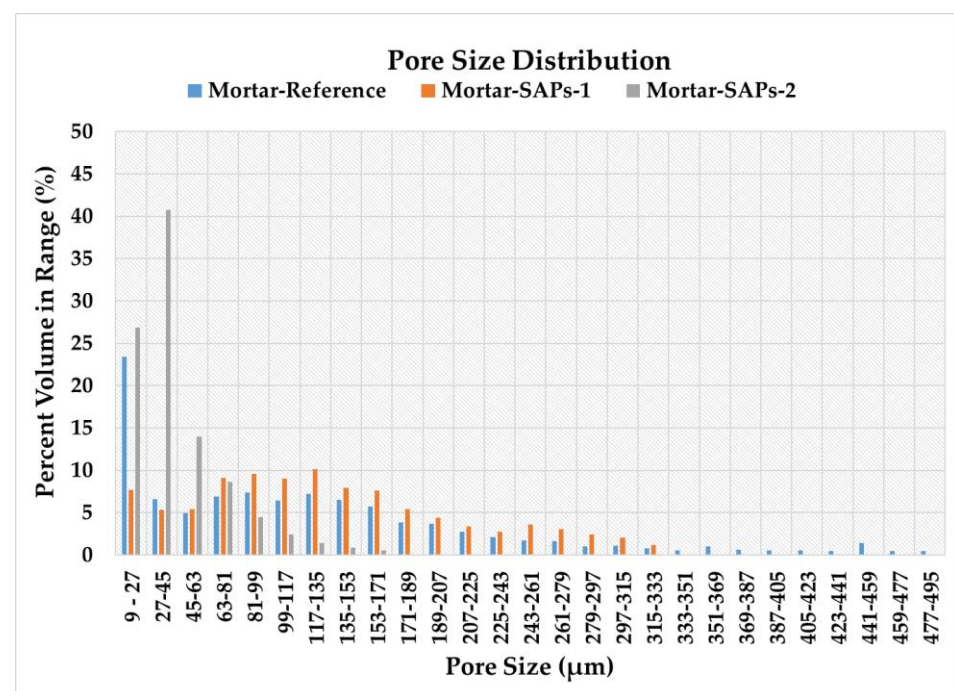| Property	Unit	Mortar-Reference	Mortar-SAPs-1	Mortar-SAPs-2
Volume of closed porosity	mm^3	10.60	1.87	1.18
Closed porosity	%	2.440	1.800	0.341
Volume of open porosity	mm^3	5.43	1.49	2.54
Open porosity	%	1.230	1.420	0.725
Volume of total porosity	mm^3	16.10	3.36	3.72
Total porosity	%	3.64	3.19	1.06

Figure 7. Pore size distribution in mortar-reference, mortar-SAPs-1 and mortar-SAPs-2.

- "Volume of closed porosity" (mm^3) is the total volume of all closed pores within the Volume of Interest (VOI), when a closed pore in 3D is a connected assemblage of space (black) voxels that is fully surrounded on all sides in 3D by solid (white) voxels.
- "Closed porosity" (%) is the volume of closed pores (as defined above) as a percent of the total of solid plus closed pore volume, within the VOI.
- "Volume of open porosity" (mm^3) is the total volume of all open pores within the VOI. An open pore is defined as any space located within a solid object or between solid objects, which has any connection in 3D to the space outside the object or objects.

- "Open porosity" (%) is the volume of open pores (as defined above) as a percent of the total VOI volume
- "Volume of total porosity" (mm^3) is the total volume of all open and closed pores within the VOI
- "Total porosity" (%) is the volume of all open plus closed pores (as defined above) as a percent of the total VOI volume.

3.2.2. Image Segmentation and Phase Identification

There are a number of different approaches on the matter of image segmentation and phase identification via microCT Analysis. One that stands out as it is widely used is the global thresholding method in GSH. The GSH with the Gaussian deconvolution procedure performed for the mortars examined in this work, are given in Figure 8.
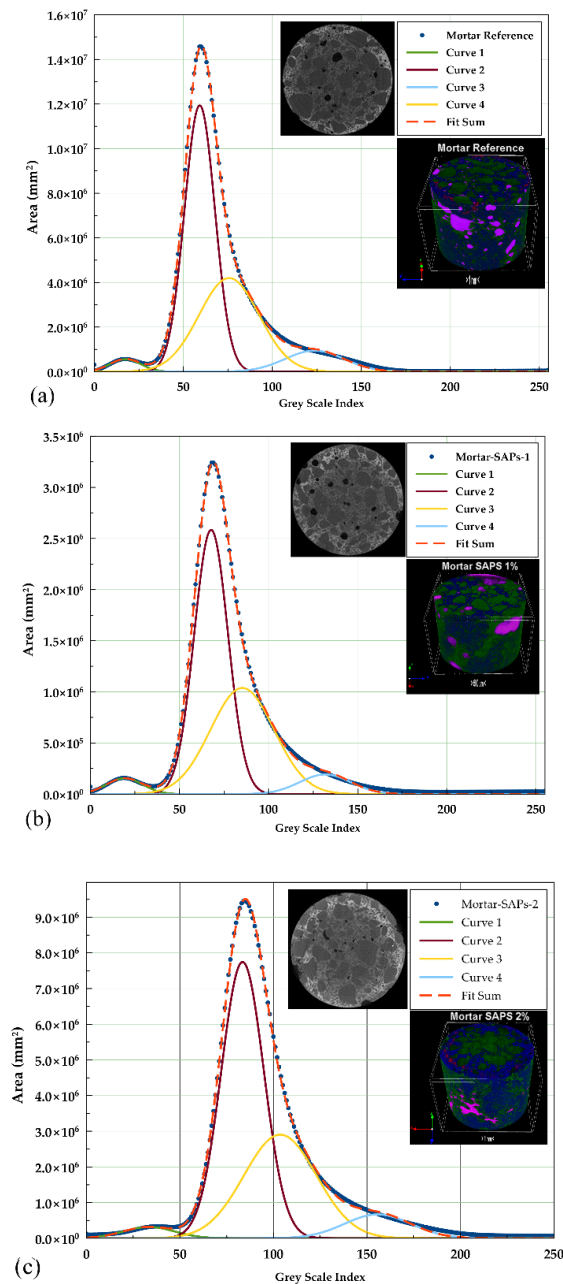

Figure 8. Grey Scale Histogram with the Gaussian deconvolution fit for mortar-reference (**a**), mortar-SAPs-1 (**b**), mortar-SAPs-2 (**c**).

The deconvolution of the initial GSH as described earlier, produced four distinct curves in each case, curves 1 to 4 and the corresponding peaks (Figure 8). Curve 1—Peak 1 were attributed to pores, curve 2 and curve 3 were assigned to hydrated cement phases and curve 4 was ascribed to unhydrated cement phases and SAPs. We observed that for all specimens the main peak in the GSH was deconvoluted in two separate peaks which were attributed to different hydrated products probably owed to the main hydrated cement products which are Calcium Silicate Hydrates, C-S-H and Calcium Hydroxide, $Ca(OH)_2$.

Then, using the GSH data, the quantitative determination of the different phases identified in the mortar specimens was performed and the corresponding results were tabulated in Table 4. Taking into consideration the data in Table 4, it is observed that in the case of mortar-SAPs-1 the unhydrated cement products together with the incorporated SAPs (1% bwoc) represented only the 5% of the total material when the corresponding values for both mortar-reference and mortar-SAPs-2 were 36%. This indicates that the progress of the hydration reactions for this material was remarkably enhanced compared to mortar-reference and mortar-SAPs-2, as a result of SAPs incorporation in the cementitious matrix. This is attributed to more effective SAPs dispersion in the cementitious matrix and therefore enhancement of their functionality to extend hydration reactions during cement curing, thus promoting this as the optimal SAPs concentration in mortars in respect to microstructure evaluation.

Table 4. Quantitative determination of the different cement phases identified in the mortars.

% Phase	Mortar-Reference	Mortar-SAPs-1	Mortar-SAPs-2
Peak 1	2	3	3
Peak 2	54	54	55
Peak 3	8	38	7
Peak 4	36	5	36

3.2.3. Self-Healing Evaluation

In Figure 9 the crack surface and the larger voids in respect to cracks and large holes in the bulk of the specimens immediately after they were cracked (0 days) and after 8 days of healing treatment, are shown for the mortar specimens examined in this work.
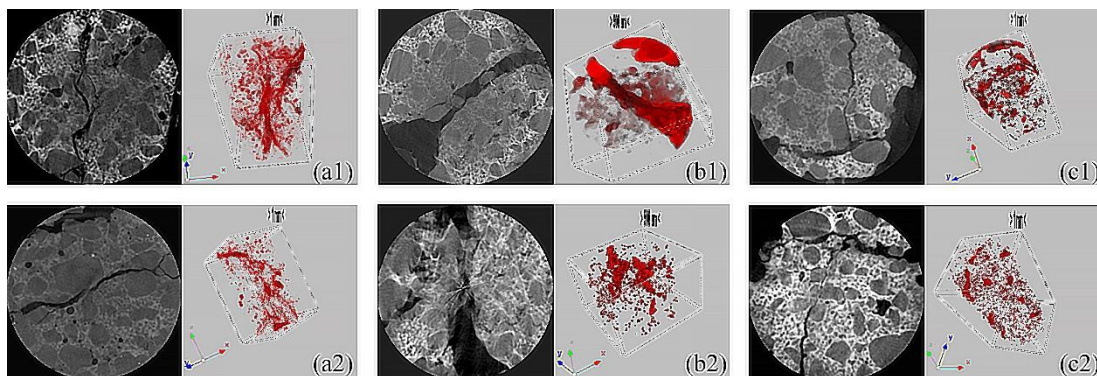

Figure 9. Initial microCT images depicting voids (in respect to both large pores and cracks) in red color for mortar-reference ($\mathbf{a_1}$), mortar-SAPs-1 ($\mathbf{b_1}$) and mortar-SAPs-2 ($\mathbf{c_1}$) and corresponding images after 8 days of healing treatment for mortar-reference ($\mathbf{a_2}$), mortar-SAPs-1 ($\mathbf{b_2}$) and mortar-SAPs-2 ($\mathbf{c_2}$).

MicroCT imaging allows both to visualize the self-healing process, but also to quantitatively analyze it in terms of changes in morphology and density using methods and functions embedded in CTAnalyzer software properly adjusted for mortar specimens. The methodology followed in this work is described as follows.

The region surrounding a crack is rich in products with a vast variety of thicknesses ranging from thick intact mortar to fresh self-healing products that can be thinner or

thicker structures. Binarizing or segmenting the structures in this region can therefore be compromised. An effective solution, which has the effect of artificially diminishing the attenuation of thin structures, is the method of adaptive thresholding in CTAnalyzer custom processing procedure. Then, the (Region of Interest) ROI shrink-wrap and stretch over holes functions were performed. As a result, the (Volume of Interest) VOI was wrapped around the boundary of complex and porous objects such as thin self-healing products and the wrapped VOI was prevented from penetrating into the porous spaces of the object but instead only the complex outer margins were marked. Figures 10 and 11 depict the resulting banalization-segmentation images after applying the adaptive thresholding method and shrink-wrap function for mortar-reference, mortar-SAPs-1 and mortar-SAPs-2 specimens at 0 and 8 days of healing treatment, accordingly.
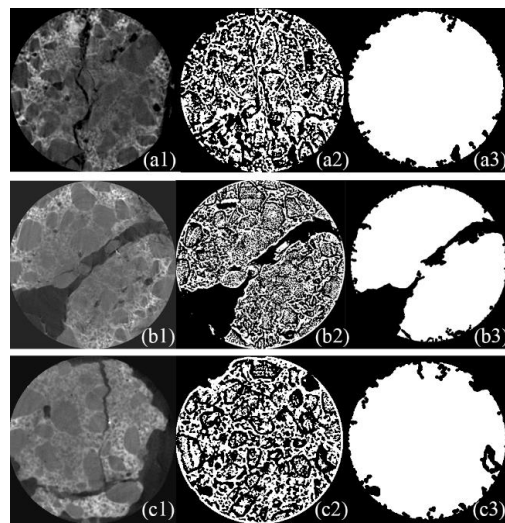

Figure 10. Initial microCT images for mortar-reference (a_1), mortar-SAPs-1 (b_1) and mortar-SAPs-2 (c_1), resulting images for mortar-reference (a_2), mortar-SAPs-1 (b_2) and mortar-SAPs-2 (c_2) and ROI images for mortar-reference (a_3), mortar-SAPs-1 (b_3) and mortar-SAPs-2 (c_3) after adaptive thresholding method and shrink-wrap function are applied before healing treatment.

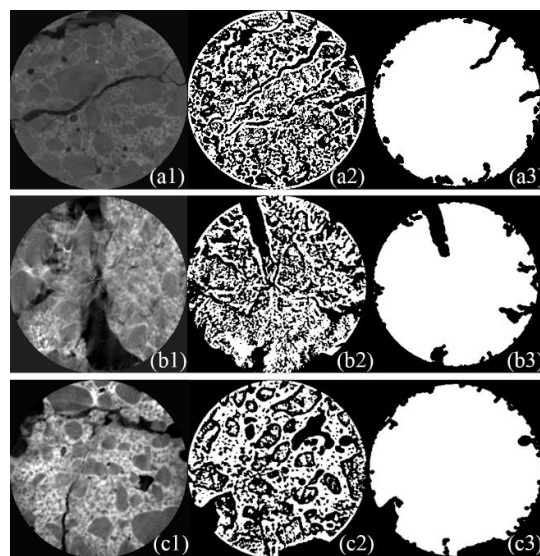**Figure 11.** Initial microCT images for mortar-reference (a_1), mortar-SAPs-1 (b_1) and mortar-SAPs-2 (c_1), resulting images for mortar-reference (a_2), mortar-SAPs-1 (b_2) and mortar-SAPs-2 (c_2) and ROI images for mortar-reference (a_3), mortar-SAPs-1 (b_3) and mortar-SAPs-2 (c_3) after adaptive thresholding method and shrink-wrap function are applied after 8 days of healing treatment.

Then, a full 3D analysis was run. The morphometric parameters calculated to quantitatively evaluate self-healing of the cracked mortar specimens were (a) percent object volume (%) and (b) connectivity density (mm^{-3}) [51,57,58]. The first parameter shows the specimen volume variations, while the second one is sensitive to structure complexity changes versus healing time. The corresponding results are shown in Figure 12.
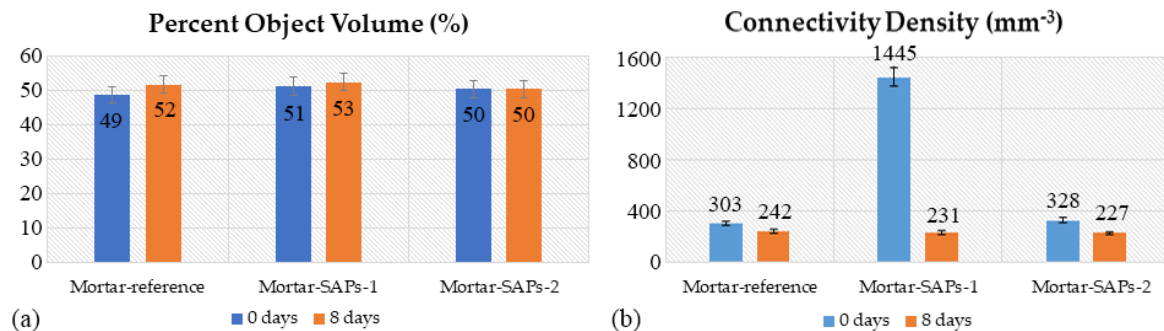

Figure 12. Calculated morphometric parameters to evaluate the self-healing process of mortars. Percent object volume (**a**), connectivity density (**b**). The error bars refer to percent error.

4. Discussion

The overall effect of SAPs incorporation in cementitious materials highly depends on the SAPs properties. In this study, in house synthesized SAPs were used with tailored properties [39]. Firstly, different SAP particle sizes introduce different effects. For the same SAP concentration and w/c ratio, the larger the SAP particle size, the lower the determined strength was in means of flexural and compressive strength. This is directly correlated with the formation of larger SAP voids left behind in the cement structure when SAPs release the amount of water they absorbed during mixing [21]. The size of the SAPs used in this work laid in the submicron scale as shown in Figure 1c, whereas the particle sizes of SAPs tested by other researchers were several micrometers [8–10,15,18,21,23].

Additionally, SAPs chemical constitution triggers different behaviors in the cementitious matrix. As mentioned earlier, most commercially available SAPs are copolymeric networks based on acrylic acid or acrylamide that may or may not have been partially neutralized [10,11,14,15,17,18,20–23,31,35] which present a low affinity with cement and as a result form large aggregates when incorporated in it. In this work, SAPs that have been tested had a hybrid organic core—inorganic shell structure. The introduction of an inorganic coating on the organic SAP core has been proposed by Kanellopoulou I. et al. (2019), via the encapsulation of the polymeric core with an inorganic CaO-SiO$_2$ shell via solution-gelation technique [31]. Other research groups have investigated the behavior of coated SAPs via the Wurster process but the compensation of the strength reduction achieved was only partial [9].

On the contrary, as indicated by the total porosity reduction and the fact that no mechanical strength degradation was determined with respect to flexural and compressive strength for the mortar/SAPs composite materials, the tailored SAPs in this work presented enhanced chemical affinity with the cementitious matrix. More specifically, due to the enhancement of the chemical affinity between SAPs and cement, large SAP agglomerates were not formed and as a result the size of the SAP voids (porosity) when water was released from their particles were smaller. Additionally, the limited water absorption capacity of the coated SAPs compared to the corresponding capacity of the uncoated particles also favored the size limitation of the SAP voids. The total porosity reduction in both cases of SAPs incorporation in mortars as shown in Table 3 indicates that:

- SAPs were homogeneously dispersed in mortars due to enhanced chemical affinity with the cementitious matrix and

- SAPs promoted hydration reactions in the cement matrix, thus forming denser and consequently more durable structures, since stress inducing points (voids) in the cement matrix were smaller. This is coherent with the mechanical properties behavior discussed later.

The slight flexural strength increment (~3%) of the mortar-SAPs specimens in comparison to the control specimens was evaluated taking into account as corroborating evidence the aforementioned porosity parameters and was attributed to the water absorbed by SAPs during the mixing process, which became available later during cement curing, thus promoting and accelerating hydration reactions. The space surrounding SAP particles was enriched with hydrated cement phases. As a result, mitigation of autogenous shrinkage and early age cracking were observed, while the densification of the cement microstructure led to the enhancement of the mortar/SAPs composites flexural strength [8,52,54,59].

Moreover, compressive strength is considered a key concrete property since it is directly correlated with concrete quality. Nevertheless, it must be clarified that the determined value of each measurement set highly depends on a variety of parameters namely the w/c, additives incorporation and curing conditions, i.e., humidity levels and temperature profiles. Curing conditions can affect drastically the compressive strength of a cementitious material. More specifically, compressive strength degradation has been correlated with low moisture levels during the first day of curing or high temperatures in the initial curing state which is responsible for lower quality hydration products [52]. Furthermore, w/c ratios used in mortars formulation have also been directly correlated with the voids formed in the concrete matrix and consequently with their mechanical strength. More specifically, increased w/c ratios have been known to lead to increased voids in the cementitious matrix and thus to the degradation of mechanical properties [1]. The w/c ratio used in this work (0.5) is high compared to the corresponding ratios examined by other research groups. For example the w/c ratios in cementitious composites with SAPs were 0.30–0.35 in the research of Sun et al. [8], 0.40 and 0.50 in the research of De Belie et al. [9], 0.30, 0.40, 0.50 in the research of Lee et al. [10], 0.35, 0.40 and 0.50 in the research of Farzanian et al. [15] and 0.40 in the research of Kim [54]. Nonetheless, since the effective w/c ratio is not the same as the total w/c ratio, when SAPs are incorporated in mortars, excess of water must be added to counterbalance the amount of water absorbed by SAPs. Considering the dosage of SAPs used in this work (1 and 2% bwoc) the high w/c ratio of 0.50 was chosen. The w/c ratio chosen combined with the curing conditions of the mortar specimens and notably, low moisture during the first day after casting as well as low temperature during the 28 days specimen curing the value of the compressive strength of the control specimens was calculated below 52.5 MPa.

In literature, it is often reported that cementitious materials containing SAPs show poorer compressive performance compared to the corresponding materials without SAPs during all curing periods and for SAPs dosages even lower than those examined in this work, while this behavior became more pronounced for increased SAPs dosages. [1,7,9,10,15,17]. On the contrary, in this work compressive strength was not influenced by the SAPs incorporation in mortars.

The relationship between the determined flexural and compressive strength for the mortar specimens as depicted in Figure 6 was also indicative of the fact that SAPs incorporation in the mortars affected flexural and compressive strength in a similar manner and that their incorporation did not negatively influence the mortar microstructure and hence the mortar strength was not degraded [53,54].

According to the results in Table 3, the percentage of total porosity was reduced by 0.5% and 2.5% in the cases of mortar-SAPs-1 and mortar-SAPs-2, respectively. Moreover, the percentage of open porosity was also reduced in the case of mortar-SAPs-2 compared to mortar-reference by 0.5%. Open porosity represents the pores which are in direct contact with the specimen environment thus allowing humidity and/or other harmful factors (e.g., corrosive factors) to penetrate the bulk of the specimen and cause the material

deterioration. As a result, the open porosity reduction in cementitious materials promotes their mechanical integrity and their sustainability.

Additionally, as shown in Figure 7, the size of the pores in the mortar-reference specimens was greater than that of the mortar-SAPs-1 and mortar-SAPs-2 specimens, while the smallest pores were recorded in the case of mortar-SAPs-2. The pore sizes in the mortar-reference specimens showed a wide distribution ranging from 9 to almost 500 μm. On the contrary, the pore sizes in mortar specimens in which SAPs had been incorporated showed a narrower distribution ranging from 9 to 333 μm and from 9 to 171 μm for mortar-SAPs-1 and mortar-SAPs-2, respectively. The more uniform the pore profile the more homogeneous the materials, which is consistent with improved mechanical properties.

Furthermore, the Gaussian deconvolution procedure of the GSH of all the mortar specimens examined in this work, showed that the minimum unhydrated cement phases (5%) were found in the case of the mortar-SAPs-1 specimens, whereas the corresponding phases in mortar-reference (36%) and mortar-SAPs-2 (35%) were almost identical (see Table 4). Firstly, this indicates that SAPs were more homogeneously dispersed in the cementitious matrix for the concentration of 1% bwoc thus allowing them to function as water reservoirs and cement hydration promoting agents and therefore led to denser and more durable cementitious structures. Secondly, it is safe to assume that even greater SAPs concentrations, if needed to render different functionalities to the mortars, will not compromise the mortar behavior.

In mortars, apart from one single crack several other microcracks are formed and distributed in the bulk of the specimens, when they are subjected to compressive loads, which sometimes may not be easy to detect using conventional methods. On the contrary, by running a full 3D analysis via microCT, apart from crack healing, the 3D volume of the specimen was also be thoroughly evaluated. As mentioned earlier, the quantitative analysis of the self-healing progress in pre-cracked mortar specimens took place via microCT Analysis. More specifically, a morphological and an architectural parameter were calculated for all mortar specimens before and after eight days of healing treatment. These parameters were:

- Morphometric parameter, "Percent Object Volume" (%) which shows the percent of the specimen volume variation during the healing treatment. The value of this parameter increases with healing time, since healing products that are formed cover progressively the crack volume in part, thus representing the healing progress with time [51,57,58].
- Architecture parameter, "Connectivity Density" (mm^{-3}) comprising a sensitive indicator of the change in texture and complexity associated with the healing progression. More specifically Connectivity Density is an indicator of complex, very highly porous structures. The value of this parameter decreases with healing time, since crack healing provides denser structures within the crack volume [58,60].

In order to estimate the relative self-healing enhancement of mortar/SAPs specimens versus the control specimens, the relative self-healing enhancement index h_i (%) was calculated [61], based on the results of Connectivity Density since this architecture parameter is very sensitive to texture and complexity changes.

$$h_i(\%) = \left(1 - \frac{CD_{i,n}}{CD_{i,0}}\right) \times 100, \tag{1}$$

where:

h_i: relative self-healing enhancement index for specimen, i

$CD_{i,n}$: value of Connectivity Density for specimen, i after n days of self-healing treatment

$CD_{i,0}$: value of Connectivity Density for specimen, i before self-healing treatment (at 0 days)

More specifically, when no self-healing is observed h_i value is "0", as the final and the initial value of connectivity density are the same. On the other hand, when self-healing is promoted, h_i values become higher and approach the value "100", since the

ratio $CD_{i,n}/CD_{i,0}$ approaches "0" as $CD_{i,n}$ decreases. The corresponding values of h_i for the mortar/SAPs and control specimens are shown in Table 5 and it is revealed that the self-healing index was 84% and 31% for mortar-SAPs-1 and mortar-SAPs-2, respectively, while it was 20% for mortar-reference specimen. Comparatively, self-healing was enhanced by about 60% and 10% for mortar-SAPs-1 and mortar-SAPs-2, respectively compared to the mortar-reference specimen. These results reveal that healing efficiency was optimized for the specimen mortar-SAPs-1. This is attributed to the more effective dispersion of SAPs in the cementitious matrix for the SAPs concentration 1% bwoc and therefore the enhancement of their functionality as self-healing agents. This conclusion is in agreement with that drawn by the phase identification in mortars via image segmentation obtained by microCT scans.

Table 5. Indexes h_i for the mortar/SAPs specimens and control specimens.

Specimen	h_i (%)
Mortar-reference	20
Mortar-SAPs-1	84
Mortar-SAPs-2	31

At this point, it must be taken into consideration that the specimen mortar-SAPs-1 was more severely damaged during the artificial inducement of the crack by the application of compressive load, leading to a very high initial value for connectivity density.

Our future goal is to expand this preliminary study on the evaluation of the self-healing behavior of mortars containing the proposed SAPs for longer treatment durations and attain a more profound insight on the healing mechanisms.

5. Conclusions

The presented work, took into consideration the overall behavior of the mortar-SAPs composites manufactured and examined. It also comprises the determination of their mechanical properties, their microstructure evaluation, as well as the evaluation of their self-healing behavior yielding a series of conclusions. Even though it is often reported in literature that the incorporation of SAPs in mortars causes degradation in mechanical properties and specifically in compressive strength [1,7,9,10,15,17], within the manuscript it is shown that, the incorporation of tailored SAPs with respect to their structure (hybrid organic core—inorganic shell structure, spherical shape in the submicron scale) did not negatively influence neither the flexural nor the compressive strength of the mortars. This is directly correlated with the microstructure and porosity evaluation of the mortars, which took place via microCT analysis. In particular, the total porosity was reduced by about 0.5% and 2.5% for mortar-SAPs-1 and mortar-SAPs-2, respectively, while the range of the pore size distribution became narrower for both SAPs concentrations compared to the control specimens. As a result, these SAPs enhanced cement hydration reactions when incorporated in the mortars without introducing more stress inducing sites (macropores left behind in the matrix because of the deswelling of SAPs particles during cement curing) and consequently not compromising the mortars strength. Moreover, the Gaussian deconvolution procedure of the GSH of all the mortar specimens examined in this work, showed that the minimum unhydrated cement phases (5%) after 28 days of aging, were found in the case of mortar-SAPs-1, which also revealed the more pronounced self-healing behavior.

Conclusively, the overall SAPs functionality in cementitious-based materials was optimized while, the SAP concentration of 1% bwoc was promoted as the premium one in reference to mortar composite strength, microstructure and self-healing enhancement.

Author Contributions: Conceptualization, I.A.K. (Irene A. Kanellopoulou) and I.A.K. (Ioannis A. Kartsonakis); methodology, I.A.K. (Irene A. Kanellopoulou); software, I.A.K. (Irene A. Kanellopoulou) and I.A.K. (Ioannis A. Kartsonakis); validation, I.A.K. (Irene A. Kanellopoulou), I.A.K.

(Ioannis A. Kartsonakis) and C.A.C.; formal analysis, I.A.K. (Irene A. Kanellopoulou) and I.A.K. (Ioannis A. Kartsonakis); investigation, I.A.K. (Irene A. Kanellopoulou); resources, I.A.K. (Irene A. Kanellopoulou) and I.A.K. (Ioannis A. Kartsonakis); data curation, I.A.K. (Irene A. Kanellopoulou); writing—original draft preparation, I.A.K. (Irene A. Kanellopoulou) and I.A.K. (Ioannis A. Kartsonakis); writing—review and editing, I.A.K. (Ioannis A. Kartsonakis) and C.A.C.; visualization, I.A.K. (Irene A. Kanellopoulou) and I.A.K. (Ioannis A. Kartsonakis); supervision, C.A.C.; project administration, C.A.C.; funding acquisition, C.A.C. All authors have read and agreed to the published version of the manuscript.

Institutional Review Board Statement: Not applicable.

Informed Consent Statement: Not applicable.

Data Availability Statement: Data sharing not applicable.

Conflicts of Interest: The authors declare no conflict of interest.

References

1. He, Z.; Shen, A.; Guo, Y.; Lyu, Z.; Li, D.; Qin, X.; Zhao, M.; Wang, Z. Cement-based materials modified with superabsorbent polymers: A review. *Constr. Build. Mater.* **2019**, *225*, 569–590. [CrossRef]
2. Zhang, W.; Zheng, Q.; Ashour, A.; Han, B. Self-healing concrete composites for sustainable infrastructures: A review. *Compos. Part B Eng.* **2020**, *189*, 107892. [CrossRef]
3. The European Cement Association (CEMBUREAU). *Activity Report*; The European Cement Association (CEMBUREAU): Belgium, Brussels, 2018; pp. 1–53.
4. Sanjuán, M.Á.; Andrade, C.; Mora, P.; Zaragoza, A. Carbon Dioxide Uptake by Mortars and Concretes Made with Portuguese Cements. *Appl. Sci.* **2020**, *10*, 646. [CrossRef]
5. Liu, J.; Shi, C.; Ma, X.; Khayat, K.H.; Zhang, J.; Wang, D. An overview on the effect of internal curing on shrinkage of high performance cement-based materials. *Constr. Build. Mater.* **2017**, *146*, 702–712. [CrossRef]
6. Ferrara, L.; Van Mullem, T.; Alonso, M.C.; Antonaci, P.; Borg, R.P.; Cuenca, E.; Jefferson, A.; Ng, P.-L.; Peled, A.; Roig-Flores, M.; et al. Experimental characterization of the self-healing capacity of cement based materials and its effects on the material performance: A state of the art report by COST Action SARCOS WG2. *Constr. Build. Mater.* **2018**, *167*, 115–142. [CrossRef]
7. Ma, S.; Huang, C.; Baah, P.; Nantung, T.; Lu, N. The influence of water-to-cement ratio and superabsorbent polymers (SAPs) on solid-like behaviors of fresh cement pastes. *Constr. Build. Mater.* **2021**, *275*, 122160. [CrossRef]
8. Sun, B.; Wu, H.; Song, W.; Li, Z.; Yu, J. Design methodology and mechanical properties of Superabsorbent Polymer (SAP) cement-based materials. *Constr. Build. Mater.* **2019**, *204*, 440–449. [CrossRef]
9. De Belie, N.; Gruyaert, E.; Al-Tabbaa, A.; Antonaci, P.; Baera, C.; Bajare, D.; Darquennes, A.; Davies, R.; Ferrara, L.; Jefferson, T.; et al. A Review of Self-Healing Concrete for Damage Management of Structures. *Adv. Mater. Interfaces* **2018**, *5*, 1800074. [CrossRef]
10. Lee, H.X.D.; Wong, H.S.; Buenfeld, N.R. Self-sealing of cracks in concrete using superabsorbent polymers. *Cem. Concr. Res.* **2016**, *79*, 194–208. [CrossRef]
11. Snoeck, D.; De Belie, N. Autogenous Healing in Strain-Hardening Cementitious Materials With and Without Superabsorbent Polymers: An 8-Year Study. *Front. Mater.* **2019**, *6*, 48. [CrossRef]
12. Sisomphon, K.; Copuroglu, O.; Fraaij, A. Application of encapsulated lightweight aggregate impregnated with sodium monofluorophosphate as a self-healing agent in blast furnace slag mortar. *HERON* **2011**, *56*, 13–32.
13. Bentz, D.P.; Weiss, W.J. *Internal Curing A 2010 State-of-the-Art Review*; National Institute of Standards and Technology: Gaithersburg, MD, USA, 2011. [CrossRef]
14. Lee, H.X.D.; Wong, H.S.; Buenfeld, N.R. Potential of superabsorbent polymer for self-sealing cracks in concrete. *Adv. Appl. Ceram.* **2013**, *109*, 296–302. [CrossRef]
15. Farzanian, K.; Pimenta Teixeira, K.; Perdigão Rocha, I.; De Sa Carneiro, L.; Ghahremaninezhad, A. The mechanical strength, degree of hydration, and electrical resistivity of cement pastes modified with superabsorbent polymers. *Constr. Build. Mater.* **2016**, *109*, 156–165. [CrossRef]
16. Snoeck, D. Superabsorbent polymers to seal and heal cracks in cementitious materials. *RILEM Tech. Lett.* **2018**, *3*, 32–38. [CrossRef]
17. Assmann, A. Physical Properties of Concrete Modified with Superabsorbent Polymers. Ph.D. Thesis, Universität Stuttgart, Stuttgart, Germany, 2013.
18. Schröfl, C.; Snoeck, D.; Mechtcherine, V. A review of characterisation methods for superabsorbent polymer (SAP) samples to be used in cement-based construction materials: Report of the RILEM TC 260-RSC. *Mater. Struct.* **2017**, *50*, 197. [CrossRef]

19. Snoeck, D.; Van Tittelboom, K.; Steuperaert, S.; Dubruel, P.; De Belie, N. Self-healing cementitious materials by the combination of microfibres and superabsorbent polymers. *J. Intell. Mater. Syst. Struct.* **2012**, *25*, 13–24. [CrossRef]
20. Snoeck, D.; Dewanckele, J.; Cnudde, V.; De Belie, N. X-ray computed microtomography to study autogenous healing of cementitious materials promoted by superabsorbent polymers. *Cem. Concr. Compos.* **2016**, *65*, 83–93. [CrossRef]
21. Ma, X.; Liu, J.; Wu, Z.; Shi, C. Effects of SAP on the properties and pore structure of high performance cement-based materials. *Constr. Build. Mater.* **2017**, *131*, 476–484. [CrossRef]
22. Mechtcherine, V. Use of superabsorbent polymers (SAP) as concrete additive. *RILEM Tech. Lett.* **2016**, *1*, 81. [CrossRef]
23. Pelto, J.; Leivo, M.; Gruyaert, E.; Debbaut, B.; Snoeck, D.; De Belie, N. Application of encapsulated superabsorbent polymers in cementitious materials for stimulated autogenous healing. *Smart Mater. Struct.* **2017**, *26*, 105043. [CrossRef]
24. Jensen, O.M.; Hansen, P.F. Water-entrained cement-based materials II. Experimental observations. *Cem. Concr. Res.* **2002**, *32*, 973–978. [CrossRef]
25. Pantelakis, S.; Kanellopoulou, I.; Karaxi, E.K.; Karatza, A.; Kartsonakis, I.A.; Charitidis, C.; Koubias, S. Hybrid superabsorbent polymer networks (SAPs) encapsulated with SiO_2 for structural applications. *MATEC Web Conf.* **2018**, *188*, 01025. [CrossRef]
26. Karatzas, A.; Bilalis, P.; Kartsonakis, I.A.; Kordas, G.C. Reversible spherical organic water microtraps. *J. Non Cryst. Solids* **2012**, *358*, 443–445. [CrossRef]
27. Van Tuan, N.; Ye, G.; van Breugel, K.; Copuroglu, O. Hydration and microstructure of ultra high performance concrete incorporating rice husk ash. *Cem. Concr. Res.* **2011**, *41*, 1104–1111. [CrossRef]
28. Wyrzykowski, M.; Ghourchian, S.; Sinthupinyo, S.; Chitvoranund, N.; Chintana, T.; Lura, P. Internal curing of high performance mortars with bottom ash. *Cem. Concr. Compos.* **2016**, *71*, 1–9. [CrossRef]
29. Jozwiak-Niedzwiedzka, D. Microscopic observations of self-healing products in calcareous fly ash mortars. *Microsc. Res. Tech.* **2015**, *78*, 22–29. [CrossRef] [PubMed]
30. Liu, F.; Wang, J.; Qian, X.; Hollingsworth, J. Internal curing of high performance concrete using cenospheres. *Cem. Concr. Res.* **2017**, *95*, 39–46. [CrossRef]
31. De Meyst, L.; Mannekens, E.; Araujo, M.; Snoeck, D.; Van Tittelboom, K.; Van Vlierberghe, S.; De Belie, N. Parameter Study of Superabsorbent Polymers (SAPs) for Use in Durable Concrete Structures. *Materials* **2019**, *12*, 1541. [CrossRef]
32. Ahmed, E.M. Hydrogel: Preparation, characterization, and applications: A review. *J. Adv. Res.* **2015**, *6*, 105–121. [CrossRef]
33. Goulis, P.; Kartsonakis, I.A.; Charitidis, C.A. Synthesis and Characterization of a Core-Shell Copolymer with Different Glass Transition Temperatures. *Fibers* **2020**, *8*, 71. [CrossRef]
34. Krafcik, M.J.; Erk, K.A. Characterization of superabsorbent poly (sodium-acrylate acrylamide) hydrogels and influence of chemical structure on internally cured mortar. *Mater. Struct.* **2016**, *49*, 4765–4778. [CrossRef]
35. Tan, Y.; Chen, H.; Wang, Z.; Xue, C.; He, R. Performances of Cement Mortar Incorporating Superabsorbent Polymer (SAP) Using Different Dosing Methods. *Materials* **2019**, *12*, 1619. [CrossRef] [PubMed]
36. Farzanian, K.; Ghahremaninezhad, A. The effect of the capillary forces on the desorption of hydrogels in contact with a porous cementitious material. *Mater. Struct.* **2017**, *50*, 216. [CrossRef]
37. Farzanian, K.; Ghahremaninezhad, A. Desorption of superabsorbent hydrogels with varied chemical compositions in cementitious materials. *Mater. Struct.* **2018**, *51*, 3. [CrossRef]
38. Farzanian, K.; Ghahremaninezhad, A. On the Interaction between Superabsorbent Hydrogels and Blended Mixtures with Supplementary Cementitious Materials. *Adv. Civ. Eng. Mater.* **2018**, *7*, 20180073. [CrossRef]
39. Kanellopoulou, I.; Karaxi, E.K.; Karatza, A.; Kartsonakis, I.A.; Charitidis, C.A. Effect of submicron admixtures on mechanical and self-healing properties of cement-based composites. *Fatigue Fract. Eng. Mater. Struct.* **2019**, *42*, 1494–1509. [CrossRef]
40. European Committee for Standardization. *Methods of Testing Cement—Part 1: Determination of Strength*; European Committee for Standardization: Belgium, Brussels, 2005; Volume BS EN 196-1, pp. 2–33.
41. Gallucci, E.; Scrivener, K.; Groso, A.; Stampanoni, M.; Margaritondo, G. 3D experimental investigation of the microstructure of cement pastes using synchrotron X-ray microtomography (μCT). *Cem. Concr. Res.* **2007**, *37*, 360–368. [CrossRef]
42. Nestle, N.; Dakkouri, M.; Geiger, O.; Freude, D.; Kaerger, J. Blastrurnace slag cements: A construction material with very unusual nuclear spin relaxation behavior during hardening. *J. Appl. Phys.* **2000**, *88*, 4269–4273. [CrossRef]
43. Wang, Y.C.; Li, Z.Y.; Wang, S.H.; Yang, W.G.; Liu, W.; Li, L.Y.; Tang, L.P.; Xing, F. Analysis methodology of XCT results for testing ingress of substances in hardened cement paste: Explained with chloride immersion test. *Constr. Build. Mater.* **2019**, *229*, 116839. [CrossRef]
44. Zhang, M.; He, Y.; Ye, G.; Lange, D.A.; Breugel, K.V. Computational investigation on mass diffusivity in Portland cement paste based on X-ray computed microtomography (μCT) image. *Constr. Build. Mater.* **2012**, *27*, 472–481. [CrossRef]
45. Deboot, J.T. Investigation of X-Ray Computed Tomography for Portland Cement Phase Quantification. Ph.D. Thesis, Oregon State University, Corvallis, OR, USA, 2018.
46. du Plessis, A.; Boshoff, W.P. A review of X-ray computed tomography of concrete and asphalt construction materials. *Constr. Build. Mater.* **2019**, *199*, 637–651. [CrossRef]
47. MacLeod, A.J.N.; Collins, F.G.; Duan, W.; Gates, W.P. Quantitative microstructural characterisation of Portland cement-carbon nanotube composites using electron and x-ray microscopy. *Cem. Concr. Res.* **2019**, *123*, 105767. [CrossRef]
48. Wyrzykowski, M.; Assmann, A.; Hesse, C.; Lura, P. Microstructure development and autogenous shrinkage of mortars with C-S-H seeding and internal curing. *Cem. Concr. Res.* **2020**, *129*, 105967. [CrossRef]

49. Guntoro, P.I.; Ghorbani, Y.; Koch, P.-H.; Rosenkranz, J. X-ray Microcomputed Tomography (μCT) for Mineral Characterization: A Review of Data Analysis Methods. *Minerals* **2019**, *9*, 183. [CrossRef]

50. Bossa, N.; Chaurand, P.; Vicente, J.; Borschneck, D.; Levard, C.; Aguerre-Chariol, O.; Rose, J. Micro- and nano-X-ray computed-tomography: A step forward in the characterization of the pore network of a leached cement paste. *Cem. Concr. Res.* **2015**, *67*, 138–147. [CrossRef]

51. Yu, N.Y.; Schindeler, A.; Peacock, L.; Mikulec, K.; Fitzpatrick, J.; Ruys, A.J.; Cooper-White, J.J.; Little, D.G. Modulation of anabolic and catabolic responses via a porous polymer scaffold manufactured using thermally induced phase separation. *Eur. Cell. Mater.* **2013**, *25*, 190–203. [CrossRef]

52. Soliman, A.M. Early-Age Shrinkage of Ultra High-Performance Concrete: Mitigation and Compensating Mechanisms. Ph.D. Thesis, University of Western Ontario, London, KY, Canada, 2011.

53. Medeiros, M.H.F.; Helene, P.; Selmo, S. Influence of EVA and acrylate polymers on some mechanical properties of cementitious repair mortars. *Constr. Build. Mater.* **2009**, *23*, 2527–2533. [CrossRef]

54. Kim, M.O. Influence of Polymer Types on the Mechanical Properties of Polymer-Modified Cement Mortars. *Appl. Sci.* **2020**, *10*, 1061. [CrossRef]

55. Pipilikaki, P.; Beazi-Katsioti, M. The assessment of porosity and pore size distribution of limestone Portland cement pastes. *Constr. Build. Mater.* **2009**, *23*, 1966–1970. [CrossRef]

56. Diamond, S. The microstructure of cement paste and concrete—-A visual primer. *Cem. Concr. Compos.* **2004**, *26*, 919–933. [CrossRef]

57. Blazejczyk, A. Morphometric Analysis of One-Component Polyurethane Foams Applicable in the Building Sector via X-ray Computed Microtomography. *Materials* **2018**, *11*, 1717. [CrossRef] [PubMed]

58. Panmekiate, S.; Ngonphloy, N.; Charoenkarn, T.; Faruangsaeng, T.; Pauwels, R. Comparison of mandibular bone microarchitecture between micro-CT and CBCT images. *Dentomaxillofac. Radiol.* **2015**, *44*, 20140322. [CrossRef] [PubMed]

59. Sosa, I.; Thomas, C.; Polanco, J.A.; Setién, J.; Tamayo, P. High Performance Self-Compacting Concrete with Electric Arc Furnace Slag Aggregate and Cupola Slag Powder. *Appl. Sci.* **2020**, *10*, 773. [CrossRef]

60. Yu, Y.; Zhang, Y.X. Effect of capillary connectivity and crack density on the diffusivity of cementitious materials. *Int. J. Mech. Sci.* **2018**, *144*, 849–857. [CrossRef]

61. Ferrara, L.; Krelani, V.; Moretti, F. On the use of crystalline admixtures in cement based construction materials: From porosity reducers to promoters of self healing. *Smart Mater. Struct.* **2016**, *25*, 084002. [CrossRef]